# Integrative Biology

Accepted Manuscript






ROYAL SOCIETY OF CHEMISTRY

www.rsc.org/ibiology

Cite this: DOI: 10.1039/c0xx00000x

www.rsc.org/xxxxxx

ARTICLE TYPE

# Quantitating membrane bleb stiffness using AFM force spectroscopy and an optical sideview setup

**Carina Gonnermann[a,b], Chaolie Huang[c], Sarah F. S. Becker[c,d], Dimitar R. Stamov[a,e], Doris Wedlich[c], Jubin Kashef[c,f] and Clemens M. Franz*[a,b]**

***Received (in XXX, XXX) Xth XXXXXXXXX 20XX, Accepted Xth XXXXXXXXX 20XX***
**DOI: 10.1039/b000000x**

AFM-based force spectroscopy in combination with optical microscopy is a powerful tool for investigating cell mechanics and adhesion on the single cell level. However, standard setups featuring an AFM mounted on an inverted light microscope only provide a bottom view of cell and AFM cantilever but cannot visualize vertical cell shape changes, for instance occurring during motile membrane blebbing. Here, we have integrated a mirror-based sideview system to monitor cell shape changes resulting from motile bleb behavior of *Xenopus* cranial neural crest cells (CNCs) during AFM elasticity and adhesion measurements. Using the sideview setup, we quantitatively investigate mechanical changes associated with bleb formation and compared cell elasticity values recorded during membrane bleb and non-bleb events. Bleb protrusions displayed significantly lower stiffness compared to the non-blebbing membrane in the same cell. Bleb stiffness values were comparable to values obtained from blebbistatin-treated cells, consistent with the absence of a functional actomyosin network in bleb protrusions. Furthermore, we show that membrane blebs forming within the cell-cell contact zone have a detrimental effect on cell-cell adhesion forces, suggesting that mechanical changes associated with bleb protrusions promote cell-cell detachment or prevent adhesion reinforcement. Incorporating a sideview setup into an AFM platform therefore provides a new tool to correlate changes in cell morphology with results from force spectroscopy experiments.

## 1. Introduction

Plasma membrane blebs are spherical membrane protrusions releasing high intracellular pressure[1-5] and occur in different cell types during mitosis, cytokinesis or apoptosis[3, 6-8]. Furthermore, non-apoptotic blebbing at the leading edge has been shown to provide a mechanism for cell migration during development and metastasis[3, 9-12]. For instance, *Dictyostelium* cells produce blebs at the leading edge during amoeboid locomotion[10], while tumor cells can move using both actin polymerization-driven processes or blebbing[11, 12]. Single migrating *Xenopus* cranial neural crest (CNC) cells can temporarily switch into a tumbling mode - characterized by small randomly oriented movements and partial blebbing - while searching for a suitable migration path, after which they re-spread and migrate using non-bleb based mechanisms[13]. Zebrafish primordial germ cells (PGCs) employ bleb-like protrusions for directed migration response to chemoattractants[1]. In *Xenopus* PGCs enhanced motility also coincides with an increased formation of bleb-like protrusions[14]. In Zebrafish CNC cells underdoing epithelial-to mesenchymal-transition (EMT), membrane blebbing and loss of cell adhesion precedes filopodial extension and the onset of migration[15]. It has also been suggested that dynamic membrane blebs may suppress the formation of new cell-cell contacts so that individual cancer cells can move more efficiently through tissues[16].

Bleb nucleation can result from a local disruption of the F-actin cortex or from membrane detachment from the underlying actin cortex[1-3]. In agreement, laser ablation experiments demonstrate that blebs form locally at sites where the cell cortex is ruptured[6]. Alternatively, blebs can be initiated by changing the expression of membrane-actin linkers, such as ezrin[17, 18]. High Rho GTPase activity, a major regulator of actomyosin contractility, also stimulates bleb formation and drives bleb-based migration behaviour[19], while inhibition of myosin II or ROCK in zebrafish neural crest cells suppresses bleb formation[15]. Blebbing can be furthermore stimulated by serum addition[17, 20] or by increasing osmotic pressure[16]. During the initial growth phase (~30 sec) blebs are not stabilized by F-actin[16] and F-actin assembly occurs only after ezrin recruitment during bleb maturation, which is thought to be essential for bleb retraction typically lasting ~2 min[16, 17]. Together, these experiments demonstrate the importance of actomyosin contractility for bleb formation and retraction.

In addition to actin-mediated processes, mechanical changes occurring during bleb formation have been intensively studied. Charras *et al*. showed that total cell volume is preserved during blebbing despite the mechanical uncoupling of the plasma membrane from the cell cortex[16]. Furthermore, using flicker spectroscopy to characterize membrane bending rigidity, the

authors showed that expanding, non-actin stabilized blebs are five times softer than retracting blebs. In turn, actin depolymerizing drugs (cytochalasin D, latrunculin B) reduce membrane bending rigidity uniformly to values comparable to those of expanding blebs[16], further underlying the actin-free nature system of initial blebs.

Despite the considerable insight into mechanisms of bleb formation and function, directly probing bleb mechanics poses an experimental challenge given their fleeting nature, mechanical instability and geometric arrangement at the cell membrane. AFM-based indentation measurements have become a useful tool for investigating cell mechanics under physiological conditions [21]. AFM-based cell elasticity measurements are typically performed using pyramidal, conical or spherical microindentor probes attached to an AFM cantilever to deform cells with a defined indentation force or depth. Cell elasticity values can then be extracted from the force-distance curves using the Hertz model or other models[22]. Placing the AFM on an inverted optical microscope allows for accurate positioning of the indenter over the cell and such dual setups are used routinely in cell elasticity measurements. For analyzing dynamic modulations in membrane mechanics associated with bleb formation, ideally the stiffness of blebbing and non-blebbing cell membranes should be measured directly using the same cell. This, however, requires precise visual control during the indentation measurement to reliably distinguish blebbing and non-blebbing membranes. Unfortunately, conventional AFM setups do not permit visualizing vertical cell deformations, and therefore cannot be used to identify blebs forming at the top of the cell within the membrane zone accessible to the AFM indenter. Powerful lens-based sideview systems have been developed which can be used to monitor vertical cell shape changes with high resolution, but these systems require a customized microscope setup[23]. Here, we have used a mirror-based sideview setup to visualize spontaneous bleb formation in *Xenopus laevis* CNC cells while performing AFM indentation measurements. This setup enables us to obtain elasticity values of both blebbing and non-blebbing membranes in the same cell. Using this novel setup we quantitatively demonstrate that blebs are significantly softer than non-blebbing membranes. Furthermore, using AFM single-cell force spectroscopy in combination with the sideview setup, we show that membrane blebs forming within the cell-cell contact zone weaken cell-cell adhesion strength and promote cell detachment.

## 2. Materials and Methods

### 2.1 CNC explants

Handling of *Xenopus laevis* embryos and cranial neural crest (CNC) explants were performed as previously described [24, 25]. For isolation of single cells, CNC explants were first incubated in dissociation buffer (50 mM NaCl, 0.67 mM KCl, 18.4 mM $Na_2HPO_4$, 0.85 mM $KH_2PO_4$, 2.4 mM $NaHCO_3$, 1.8 mM EDTA, pH 7.3) for <30 s. After dissociation, single CNC cells were transferred into Danilchik's medium (53 mM NaCl, 15 mM $NaHCO_3$ 13.5 mM $Na_2CO_3$, 4.5 mM potassium gluconate, 5 mM bicine, 1 mM $CaCl_2$, 1 mM $MgSO_4$, 1% PenStrep, pH 8.3), positioned close to the edge of a fibronectin-coated glass pedestal (see below) and incubated for 30 min to establish substrate contact before commencing force spectroscopy experiments. To prepare an additional probe cell to be immobilized on an AFM cantilever for cell-cell adhesion measurements, the singularization protocol was repeated on a second CNC explant immediately before performing adhesion measurements. Mean motile bleb velocities were determined by tracking the position of the leading edge of individual bleb in timelapse images recorded in conventional view or sideview at 0.1 fps (a total of 30 blebs from three different cells were analysed).

### 2.2 Indentation measurements

Indentation experiments were performed using a JPK CellHesion 200 AFM (www.jpk.com) mounted onto an AxioObserver.A1 inverted optical microscope (www.zeiss.com). Cell indentors were prepared by gluing single silica beads (diameter ~8-10 µm, PSI-10.0, www.kisker-biotech.com) onto tipless V-shaped cantilevers (NP-O, type D, nominal spring constant 0.06 N/m, www.veeco.com) using a solvent-free, two-component epoxy resin-based adhesive (UHU Plus, www.uhu.com) as previously described[26]. Individual bead radii were approximated from transmission light microscopy images collected using an Epilan 50x/0.50 lens (www.zeiss.com). After determining the cantilever spring constant *in situ* using the thermal noise method[27], the silica bead was positioned centrally over a single cell and indentation force spectroscopy was performed with a constant piezo extension rate of 1 µm/s until reaching a preset force of 1.5 nN. Repetitive indentation measurements were performed every 20-25 s while recording optical sideview timelapse movies at an acquisition frame rate of 1 frame per second (fps). Cell elasticity values (Young´s modulus) were determined from AFM force curves by applying a Hertzian model for a spherical indenter to AFM force curves to an indentation depth of 500 nm according to the following approximation:

$$F = \frac{4}{3}\frac{E}{1-\nu^2}\sqrt{R\delta_0^3} \qquad (1)$$

Here, $F$ is the applied force, $E$ is the Young's modulus, $\nu$ is the Poisson's ratio (0.5 for a non-compressible biological sample), $R$ is the radius of the bead indenter, and $\delta_0$ is the sample indentation. Using indenter beads with $R$ ~5 µm ensured that $R$ was large compared to the indentation depth (0.5 µm).

### 2.3 Cell-cell adhesion force spectroscopy

Cell-cell adhesion force measurements we performed using a JPK CellHesion200 AFM equipped with a sideview cantilever holder (see below). Tipless AFM cantilevers were hydrophilized by plasma-activation (100 W, 5 min) and functionalized with concanavalin A (ConA, 2.5 mg/ml in phosphate buffered saline (PBS), www.sigmaaldrich.com) overnight at 4°C and afterwards carefully rinsed with PBS[28]. Functionalized cantilevers were used immediately or stored at 4°C in PBS for up to one week. SCFS measurements were performed at room temperature in Danilchik's media. A single cell suspension was prepared from dissociated CNC explants and pipetted near to the edge onto the glass-pedestal (see below). A single cell was attached to a ConA-functionalized cantilever by maintaining contact with the cell using a force of 0.5 nN for 1 s. After a recovery period of 10 min, the cantilever-attached cell was positioned over a second cell adhering to the substrate near the edge of the glass pedestal (see below). Force measurements were carried out using a contact

force of 1.5 nN, an approach speed of 1 µm/s, a contact time of 30 s, and a retract speed of 0.2 µm/s. Maximum detachment forces as a read-out of adhesion strength were extracted from the recorded force curves using the JPK DataProcessing software (www.jpk.com).

### 2.4 Sideview setup

Sideview images were obtained using a commercially available

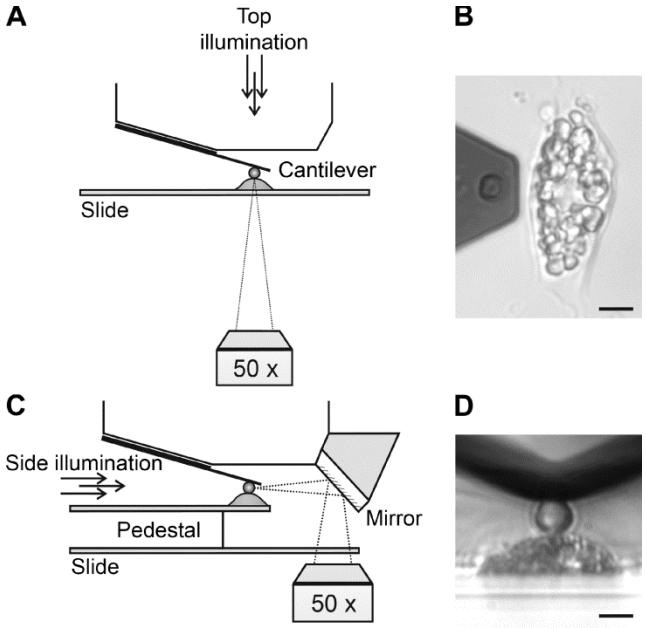


**Fig. 1** Optical sideview setup. (A) Conventional AFM setup incorporating an inverted light microscope. For indentation force measurements, a microbead is immobilized on a tipless AFM cantilever and positioned above a single target cell. (B) Brightfield image of a cantilever carrying a microbead above the target cell in standard view. (C) Mirror-based sideview setup using lateral illumination. A pedestal is necessary to prevent the overhanging sideview mirror from contacting the sample support during cantilever approach. (D) The microbead indenter immobilized on a V-shaped cantilever in contact with the target cell single cell in sideview. Scale bars in B and D correspond to 10 µm.

sideview setup (www.jpk.com). This setup features a mirror permanently attached to the AFM cantilever holder at an angle of 45 degrees (www.jpk.com). By positioning the optical axis of the optical microscope lens below the mirror, a reflected sideview image of the cantilever and the probe cell can be recorded. Sideview experiments require immobilizing the tested cells at the edge of a glass pedestal to avoid bottom contact of the sideview mirror with the sample support during cantilever approach. Using a glass-pedestal substrate increases the length of the optical path, which can be accommodated for by using a long working distance objective (Epiplan 50x/0.50, www.zeiss.com). Pedestals were constructed by gluing a ~12x8 mm piece of a microscope glass slide (www.carlroth.de) into a ∅35 mm glass bottom cell culture dish (fluorodish, www.wpiinc.com) using Dymax OP-29 optical adhesive (www.dymax.com). For curing, the adhesive was exposed to UV light (365 nm) on a Super-Bright UV table (www.vilber.de) at a power of 0.1 W/cm$^2$ for 5 min. Afterwards, a drop of the same adhesive was positioned onto the slide piece and a coverslip (12x12 mm, thickness 0.13-0.16 mm, www.menzel.de) was placed on top of the adhesive, with the long side shifted 2 mm inside relative to the slide piece. The adhesive was again cured with UV-light. All glass components of the pedestal setup were initially cut to measure and rinsed in dd$H_2O$, 70% EtOH, and then 100% EtOH, and subsequently dried in an $N_2$ stream. Likewise, the fully assembled pedestals were washed and dried using the same protocol. Before starting force spectroscopy experiments, the pedestal was coated without additional surface activation with 50 µl bovine fibronectin (50 µg/ml, www.sigmaaldrich.com) for 1 h at room temperature, washed twice with PBS and Danilchik´s medium. The substrate was used immediately or stored up to one day at 4°C in Danilchik´s medium. During force spectroscopy the cantilever carrying the immobilized bead was approached to a height of ~20 µm above the cell. The light microscopy setup was then switched from standard to sideview by positioning the sideview mirror above the optical axis of the microscopy objective. The sample support was moved by a corresponding distance to ensure a similar position of the cantilever in regard to the target cell. The mechanical stability of the setup was sufficient for both elasticity and adhesion measurements and comparable to glass bottom dishes without pedestals. Sideview illumination was provided by a 150 W gooseneck lamp (www.schott.com). Images were collected using a Zeiss Axiocam MRm camera and the AxioVison rel. 4.7 software (www.zeiss.com).

### 2.5 Statistical Analysis

Statistical analysis was performed using GraphPad Prism 5 software (www.graphpad.com). Elasticity values were plotted as mean ± SD or as box-whisker plots. Statistical significance was tested with a nonparametric Mann-Whitney test. Statistical significance with p-values < 0.05 is indicated with a star.

## 3. Results and discussion

### 3.1 Incorporating an optical sideview into an AFM setup

AFM-based force spectroscopy is a useful tool for investigating mechanical and adhesive properties of surface-attached cells. In these measurements cells are usually contacted by the AFM cantilever from above, limiting the accessible area to the apical side of the cell. To correlate adhesive or mechanical information gained in AFM measurements with cell morphology, it would be desirable to assess the exact shape of the contact area on the apical cell membrane. For instance, when studying cells displaying bleb behavior, it would be advantageous to monitor the formation of blebs at the apical cell membrane during indentation force spectroscopy. However, standard AFM systems for biological applications usually incorporate an inverted light microscope (Fig. 1A), which only permits observing cantilever and probe cell in "bottom view" without well-resolved optical information in vertical direction (Fig 1B). To generate a "sideview" of a probe cell and the AFM cantilever during force spectroscopy, we used a commercially available cantilever holder carrying a mirror mounted at a 45 degree angle relative to the cantilever. Since the mirror protrudes ~1 mm below the cantilever tip, a glass pedestal carrying the probe cell is needed to prevent the sideview mirror from crushing into the support during cantilever approach. During force spectroscopy experiments, a tipless AFM cantilever carrying a microbead indenter is first

positioned centrally above a target cell using the conventional "bottom view" mode for visual inspection and approached until a distance of ~20 µm above the cell. The cantilever holder is then shifted laterally until the sideview mirror is positioned above the optical axis of the microscope lens. To retain the initial position of the cantilever relative to the probe cell, the support carrying the pedestal and the immobilized probe cell must be moved by an equal distance (Fig. 1C). Best results were obtained when the cantilever and the pedestal were moved alternatingly in two consecutive steps of ~0.5 mm each, followed by several smaller alternating adjustment steps. Focusing on the probe cell in sideview mode requires an objective with a long working-distance to compensate for the increased optical path via the mirror. Illumination in sideview can be provided by a gooseneck lamp serving as an external side light source (Fig. 1C). This setup provides a high quality head-on view of the indenter bead on the cantilever and the probe cell (Fig. 1D). Positioning the probe cell close to the pedestal edge (within 20 µm or so) minimizes the out-of-focus contribution of the pedestal edge and thus ensures high image quality.

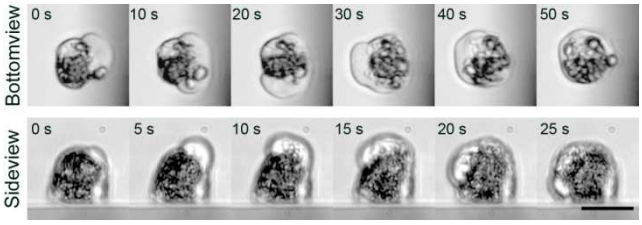


**Fig. 2** Motile membrane blebbing of CNC cells. Brightfield time-lapse imaging of a single CNC cell in conventional view visualizes clock-wise circus bleb movement in horizontal orientation (upper image row). Sideview images demonstrate bleb movement in vertical direction (lower image row). Scale bar 20 µm. The complete timelapse series are contained in Video S1.

### 3.2 Visualizing vertical and horizontal blebbing in CNC cells

Cranial neural crest (CNC) cells from *Xenopus laevis* are a multipotent and highly migratory cell population[29]. CNC cells freshly explanted onto a fibronectin substrate display a strong blebbing phenotype, which gradually reduces as cells spread fully over the time course of 1 to 3 hours. Their inherent blebbing behavior without a need for mechanical or chemical stimulation make CNC cells a useful *in vitro* model system to investigate mechanical changes occurring during blebbing. Time-lapse imaging of single CNC cells in conventional light microscopy mode revealed perpetual circular bleb movement around the cell perimeter with velocities between 0.2 and 1.5 µm/s (mean velocity ~0.7 µm/s), in agreement with previous observations[16]. Blebs were identified as round cellular protrusions free of granular yolk platelets, which are small opaque cytosolic compartments typical for *Xenopus* cells. Individual blebs frequently move around the cell several times before being retracted and disassembled. The changing position of the granular platelets revealed active flow of cytosol and cellular compartments into the bleb volume (Fig. 2, top row and Video S1). Such cytosolic flow in combination with asymmetrical F-actin polymerization has been suggested to drive lateral circus movement of blebs[17]. However, time-lapse imaging of the same cell in sideview mode showed that blebs also move around the cell in vertical direction (Fig. 2, bottom row, and Video S1). Thus, bleb formation and bleb movement are not restricted to a plane parallel to the cell substrate. The typical influx of granular platelets was also visible in sideview mode and vertical blebs moved at similar speed ($0.9 \pm 0.3$ µm/s) as horizontal blebs ($0.7 \pm 0.3$ µm/s), indicating that horizontal and vertical blebs are functionally and mechanically equivalent (Fig. 2 and Video S1). Furthermore, we frequently observed bleb movement changing from a horizontal to a vertical direction.

### 3.3 Characterizing mechanical changes during bleb formation

Blebs forming at the top of surface-attached CNC cells could be identified for the first time using the sideview setup, enabling us to investigate bleb mechanics using vertical AFM indentation spectroscopy. By performing repeated indentation measurements on blebbing and non-blebbing membranes of the same cell, we investigated whether dynamic membrane blebbing correlates with transient differences in membrane mechanics. Due to the stochastic pattern of bleb formation and the high velocity and frequently changing direction of bleb movement, indentation measurements could not be targeted to blebbing membranes directly. Instead, we performed continuous indentation measurements every 20-25 s on individual cells while monitoring bleb behaviour in sideview. Indentation measurements were then grouped manually into bleb events (indenter pushed on top of a membrane bleb) and non-bleb events (indenter pushed onto a non-blebbing membrane). This approach allowed for a direct comparison of mechanical changes during bleb formation in the same cell. Cell elasticity values (Young´s moduli) were then obtained by applying a Hertz fit to the indentation force curves to a constant indentation depth of 500 nm At this indentation depth, Hertz model fitting of bleb and non-bleb indentation curves yielded similar fit goodness values, indicating the general applicability of the Hertz model to blebbing membranes despite the absence of a cortical actin cytoskeleton in this case. The 500 nm indentation depth is also far smaller than the typical cell diameter (15-20 µm) or the mean bleb thickness (5-10 µm), avoiding potential contributions of the supporting glass substrate or non-bleb-associated cellular structures to the obtained elasticity values. Indentation measurements performed on non-blebbing membranes yielded an average Young´s modulus (mean ± SD) of 270 ± 140 Pa (Fig. 3A). By comparison, blebbing membranes were significantly softer (170 ± 120 Pa, Fig. 3A). Actomyosin-based contractility provides a major contribution to cell cortex tension. For instance, inhibiting myosin II reduces cortical tension of mouse fibroblasts by ~50%[6]. To test whether the higher stiffness of non-blebbing membrane areas depends on the actomyosin system, we inhibited myosin II activity by adding blebbistatin (50 µM). Blebbistatin treatment fully arrested bleb formation within 30 min, in agreement with previous observations in other cell types[16], and reduced cell elasticity values from 270 ± 140 Pa (non-blebbing membrane, blebbistatin untreated) to 140 ± 120 Pa, or roughly by a factor of 2 (Fig. 3A). The elasticity values obtained after blebbistatin treatment were on a similar level compared to membrane blebs (140 ± 120 Pa), consistent with the largely F-actin-free architecture of blebs[16]. Thus, different Young´s modulus values of blebbing and non-

blebbing membranes result to a large degree from different degrees of actomyosin activity.

As described above, blebbing and non-blebbing membranes display significant differences in mean Young´s modulus values. However, probing single cells repeatedly revealed fluctuations in elasticity values between force cycles, both within the "bleb" and the "non-bleb" event groups (Fig. 3B). Slight cell movement between measurements could be one reason for the variation of elasticity values, leading to subtle changes in the contact regime between bead and membrane. Also, blebs pushing against the bead or moving out of the contact zone could lead to different results. Nevertheless, while the obtained stiffness range on blebbing (30-300 Pa) or non-blebbing membranes (100-400 Pa) partially overlapped, the distributions differed significantly (Fig. 3B). The relative drop in Young´s modulus during blebbing detected in the repetitive single-cell experiments (Fig. 3B) was comparable to experiments where elasticity values of bleb and non-bleb events were averaged over several cells (Fig. 3A), although individual cells displayed variations in absolute cell stiffness. With increasing indentation measurement number, cell elasticity values neither decreased nor increased systematically, demonstrating that potential mechanical stimulation provided by the measurement did not cause stiffening or softening of the cell membrane areas contacted by the bead. Likewise, the blebbing frequency remained unchanged during repetitive measurements, indicating that even repetitive indentation measurements neither stimulated nor suppressed natural bleb formation.

### 3.4 Observing dynamic changes in cell mechanics during bleb movement

In agreement with a softer membrane system, force curves obtained on blebbing membranes typically displayed lower curvature (Fig. 3C, upper panel), while force curves on non-blebbing membranes displayed increased curvature (Fig. 3C, middle panel). In some cases, however, we observed a sudden change in curvature during indentation (Fig. 3C, lower panel). Examining the corresponding frames of a simultaneously recorded timelapse movie revealed that the sudden curvature

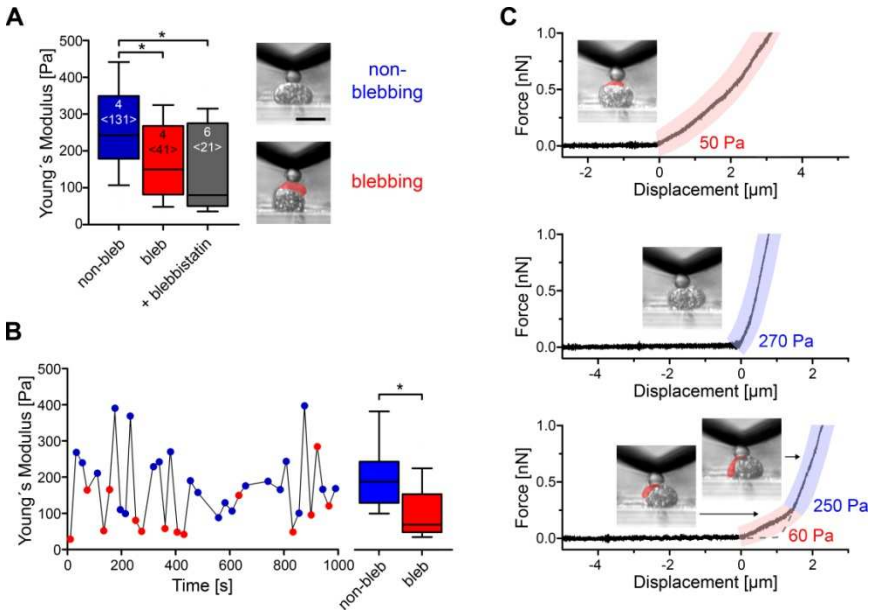


**Fig. 3** Dynamic changes in membrane stiffness during bleb formation. (A) Young´s moduli obtained by indentation measurements on non-blebbing (blue bar) or blebbing (red bar) membranes of CNC cells, and on 50 µM blebbistatin-treated cells (gray bar) displayed as box-whisker plots Number of cells tested (top) and total number of force curves (in brackets) analyzed per condition indicated within the bars. Asterisks indicate statistical significance values of $p<0.05$ (Mann-Whitney). Representative sideview images of indentation measurements on a non-blebbing (upper image) and blebbing (lower image) membrane. Scale bar 20 µm. (B) A series of indentation measurements on a single cell. From a simultaneously collected sideview timelapse recording (Video S2), indentation measurements were sorted into "bleb" (red dots) or "non-bleb" (blue dots) events. Corresponding Young´s moduli of "non-bleb" (blue bar) and "bleb" (red bar) events. The asterisk denotes a p-value <0.05. (C) Top panel: typical force curve obtained on a blebbing CNC cell and the corresponding sideview image. The membrane bleb and the segment of the force curve fitted with the Hertz-model are highlighted in red (upper panel). Middle panel: typical force curve obtained on a non-blebbing cell membrane and the corresponding sideview image. The segment of the force curve fitted with the Hertz model is highlighted in blue (middle panel). Bottom panel: force curve recorded while a motile bleb is moving out of the bead/cell contact zone during indentation. The motile membrane bleb is highlighted in red in two sideview images collected at the indicated points (arrows). A segment of the force curve with lower curvature, corresponding to bleb indentation, is highlighted in red, while a segment with increased curvature corresponding to non-blebbing membrane indentation is highlighted in blue. The dashed line indicates an interpolated Hertz fit of the steep segment. Corresponding Young´s modulus values indicated next to the respective force curve segments.

change usually correlated with movement of a single bleb out of the indenter contact zone (Fig. 3C, Video S2). Fitting the lower slope segment of the indentation force curve with the Hertz model yielded Young´s modulus values within the typical range for blebbing membranes, while applying an approximated Hertz fit to the steeper segment of the indentation force values typical for non-blebbing membranes (Fig. 3C). These results supported the interpretation that the sudden increase in membrane stiffening resulted from bleb migration away from the contact zone. The probability to observe a single bleb transit during the indentation phase depends on the bead/cell contact geometry, the indentation velocity and the bleb migration speed. Using a final indentation force of 1.5 nN and a bead indenter with a diameter of 8 µm yields a typical bead/cell contact area measuring roughly 5 µm

across. Bead-membrane contact typically lasts for ~1.5 s until the final indentation force of 1.5 nN is reached and force curve recording is terminated. Membrane blebs travelling at typical speeds of ~0.7 µm/s may therefore take several second to pass through the bead/membrane contact zone. Given the similar time scales of bead/membrane contact during indentation and bleb transit through the contact zone, observing an occasional change from blebbing to non-blebbing membrane or vice versa during a single indentation cycle is likely. Sideview indentation measurements are therefore well-suited to quantitate dynamic changes in cell cortex mechanics associated with bleb transition or bleb retraction directly.

### 3.5 Membrane blebs disrupt cell-cell adhesion

It has been previously proposed that bleb movement along the plasma membrane can lead to the breaking of adhesive bonds between neighboring cells and even cell-cell detachment[16]. In agreement, zebrafish CNC display intense membrane blebbing during delamination from the neural tube[15, 30]. Likewise, during ingression primary mesenchyme cells (PMCs) in sea urchin show strong circus bleb movement[31], which may enable them to break free from adjacent cells[32]. Blebs may also contribute to the dissolution of cell-cell interactions in cells undergoing epithelial-to-mesenchymal transition (EMT) during gastrulation[33]. Moreover, blebs could also suppress the formation of cell-cell adhesion in the first place because blebbing membranes are too dynamic to permit forming new adhesive sites between the cells[16]. However, directly quantitating the influence of blebs on cell-cell adhesion strength has been experimentally difficult and requires a sensitive technique to measure single cell adhesion forces in combination with optical monitoring of bleb position and movement.

To investigate a potential impact of membrane blebs on cell-cell adhesion strength, we performed AFM-based cell-cell adhesion force spectroscopy experiments. In these experiments a probe cell immobilized on a tipless AFM cantilever is brought into contact with a surface-immobilized cell with defined contact force and time.

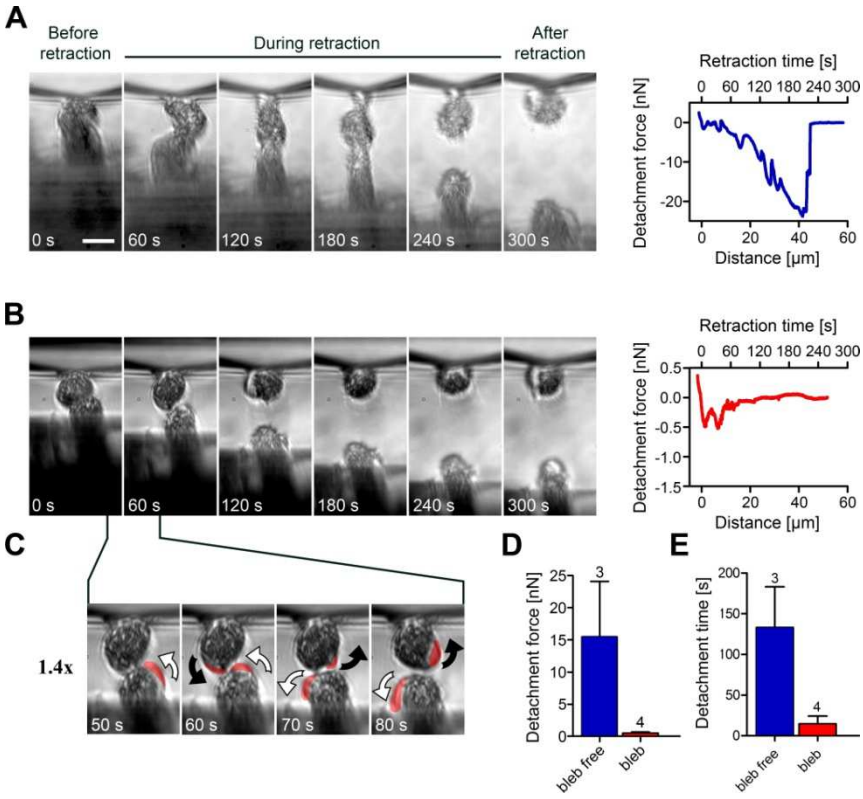


**Fig. 4** Bleb formation promotes cell-cell detachment. (A) Sideview timelapse image series of two cells separating at a 0.2 µm/s retraction speed (left side) and the corresponding force-distance curve (right side). The cell-cell contact area remains bleb-free through the separation phase. (B) Sideview timelapse image series of a cell pair detaching prematurely after bleb movement through the contact zone and the corresponding force-distance curve (right side). (C) Magnified view of images from the image series at increased frame rate (10 s) immediately before cell-cell separation. Arrows indicate antiparallel bleb movement through the cell contact zone. Blebs are highlighted in red (D) Mean cell-cell detachment forces of "bleb" and "bleb-free" groups (mean±SD). Numbers above the bars indicate the number of cell pairs tested in each experiment. The complete timelapse series is contained in Video S3.

After contact formation, the cells are separated by retracting the cantilever. The detachment force is afterwards determined from a simultaneously recorded force distance curve. These force curves typically contain a major detachment force peak (maximal detachment force) denoting overall cell-cell adhesion strength, and a series of smaller rupture force steps consistent with the sequential rupture of individual adhesive contacts prior to full cell-cell separation.

During cell-cell separation the blebbing behaviour of the cell pair was monitored using the sideview setup as described above. To increase the probability to observe blebs migrating into the cell-cell contact zone during separation, we used a retraction speed of

0.2 µm/s, which is lower than the average bleb velocity (~0.7 µm/s) along the cell perimeter. Under these conditions we observed blebs moving through the cell-cell contact region during cantilever retraction in about half of all force measurements. In case of bleb-free cell-cell separation, both cells were stretched under increasing force until they finally separated (Fig. 4A). In these cases we recorded comparatively high detachment forces of up to 25 nN. In the remaining force spectroscopy cycles, cell-cell detachment occurred under reduced cell stretching and at lower detachment force (0.5-1 nN). The corresponding sideview timelapse images usually showed one or several blebs moving into or through the cell-cell contact region just prior to cell-cell separation (Fig. 4B, Video S3), suggesting that bleb movement had contributed significantly to cell-cell separation. Quantitating cell-cell detachment forces showed significantly lower forces in the "bleb" group compared to the "bleb-free" group (Fig. 4D). Bleb transit during cell retraction also decreased the cell-cell separation time (time between the start of cantilever retraction and completion of cell-cell separation, Fig. 4E). The correlation between bleb transit though the cell-cell contact zone and low adhesion strength indicated that motile bleb transition through the cell-cell contact zone decreases cell-cell adhesion strength, possibly by "shearing" adhesive bonds between the cells or by uncoupling adhesion receptors from the cytoskeleton. Bleb formation could therefore also be one mechanism by which cells delaminate from compact cell sheet for starting individual migration, for instance during CNC cell migration or cancer metastasis. Likewise, membrane blebs may reduce attachment to other cells during individual cell migration through tissues. For instance, *Xenopus* PGCs display bleb-based migration at a velocity of 0.03 µm/s[1]. The bleb velocity of 0.7 µm/s in these cells is 20-100 times higher than their natural migration speed and blebs would therefore be expected to pass cell-cell contact zones continuously during migration.

## 4. Conclusion

Incorporating a sideview setup offers new possibilities for correlating mechanical with morphological changes during AFM-based force spectroscopy experiments. To investigate mechanical changes during motile bleb formation, indentation force spectroscopy can be performed while monitoring bleb formation, providing a reliable way for distinguishing between bleb and non-bleb events in the same cell. The results demonstrate that the Young´s Modulus of a non-blebbing membrane (270±140 Pa) is ~100 Pa higher compared to a blebbing membrane (170±120 Pa). The stiffness of the blebbing membrane was comparable to values obtained on blebbistatin-treated cells (140±120 Pa), consistent with the absence of a functional actin cytoskeleton in bleb protrusions. To investigate a potential effect of bleb protrusions on cell-cell adhesion, we also performed cell-cell adhesion force spectroscopy experiments using a lower retraction speed (0.2 µm/s) compared to the speed of bleb movement (0.7 µm/s). Under these conditions, blebs frequently passed through the cell-cell contact area during cell separation, which correlated with premature adhesion rupture and low cell-cell detachment forces. In the absence of blebs in the cell-cell contact zone, cells deformed strongly during retraction until separating at high detachment force. In conclusion, AFM measurements performed in sideview mode demonstrate different mechanical properties of non-blebbing and blebbing membranes and demonstrate a detrimental effect of motile membrane blebs on cell-cell adhesion.

## Acknowledgements

We acknowledge financial support from the Deutsche Forschungsgemeinschaft (DFG) and the State of Baden-Württemberg through the DFG-Center for Functional Nanostructures (CFN) within subproject E2.4. DW, JK, CG, CH, SFSB and CMF were also supported by DFG-FOR grants FR 1756. JK received financial further support from the ''Concept for the Future'' of the Karlsruhe Institute of Technology within the framework of the German Excellence Initiative. SB was also supported by DFG grant WE-1208-13-1.

## Notes and references

[a] *Karlsruhe Institut of Technology (KIT), Center for Functional Nanostructures, Wolfgang-Gaede-Strasse 1a, 76131 Karlsruhe, Germany. Fax: +49 (0)721 60848496; Tel: +49 (0)721 60845804; E-mail: clemens.franz@kit.edu*

[b] *Karlsruhe Institute of Technology (KIT), Zoological Institute, Department of Cell- and Neurobiology, Haid-und-Neu-Straße 9, D-76131 Karlsruhe, Germany. Fax: +49 (0)721 60848496; Tel: +49 (0)721 60845804; E-mail: clemens.franz@kit.edu*

[c] *Karlsruhe Institute of Technology (KIT), Zoological Institute, Department of Cell and Developmental Biology, Kaiserstr. 12, D-76131 Karlsruhe, Germany. Fax: +40 (0)721 60828677; Tel: +49 (0)721 60828669; E-mail: jubin.kashef@kit.edu*

[d] *Current address: Institut de Génétique et de Biologie Moléculaire et Cellulaire (IGBMC), CNRS UMR7104, INSERM U964, Université de Strasbourg, 1 rue Laurent Fries, 67404 Illkirch Cu, Strasbourg, France. Fax: +33 388 653201; Tel: +33 388 653389; E-mail: beckers@igbmc.fr*

[e] *Current address: JPK Instruments AG, Bouchéstrasse 12, 12435 Berlin, Germany. Fax: +49 (0)30 533122555; Tel: +49 (0)30 533112070; E-mail: stamov@jpk.com*

[f] *Karlsruhe Institute of Technology (KIT), Institute for Photon Science and Synchrotron Radiation, Hermann-von-Helmholtz-Platz 1, 76344 Eggenstein-Leopoldshafen, Germany. Fax: +40 (0)721 60828677; Tel: +49 (0)721 60828669; E-mail: jubin.kashef@kit.edu*

† Electronic Supplementary Information (ESI) available: [details of any supplementary information available should be included here]. See DOI: 10.1039/b000000x/

1. H. Blaser, M. Reichman-Fried, I. Castanon, K. Dumstrei, F. L. Marlow, K. Kawakami, L. Solnica-Krezel, C. P. Heisenberg and E. Raz, *Dev Cell*, 2006, **11**, 613-627.
2. E. K. Paluch and E. Raz, *Curr Opin Cell Biol*, 2013.
3. G. Charras and E. Paluch, *Nature reviews. Molecular cell biology*, 2008, **9**, 730-736.
4. A. J. Ridley, *Cell*, 2011, **145**, 1012-1022.
5. B. Maugis, J. Brugues, P. Nassoy, N. Guillen, P. Sens and F. Amblard, *J Cell Sci*, 2010, **123**, 3884-3892.
6. J. Y. Tinevez, U. Schulze, G. Salbreux, J. Roensch, J. F. Joanny and E. Paluch, *Proc Natl Acad Sci U S A*, 2009, **106**, 18581-18586.
7. J. Boss, *Exp Cell Res*, 1955, **8**, 181-187.
8. C. A. Erickson and J. P. Trinkaus, *Exp Cell Res*, 1976, **99**, 375-384.
9. D. Di Vizio, J. Kim, M. H. Hager, M. Morello, W. Yang, C. J. Lafargue, L. D. True, M. A. Rubin, R. M. Adam, R. Beroukhim, F. Demichelis and M. R. Freeman, *Cancer Res*, 2009, **69**, 5601-5609.
10. K. Yoshida and T. Soldati, *J Cell Sci*, 2006, **119**, 3833-3844.

11. E. Sahai and C. J. Marshall, *Nat Cell Biol*, 2003, **5**, 711-719.
12. K. Wolf, I. Mazo, H. Leung, K. Engelke, U. H. von Andrian, E. I. Deryugina, A. Y. Strongin, E. B. Brocker and P. Friedl, *J Cell Biol*, 2003, **160**, 267-277.
13. E. Theveneau, L. Marchant, S. Kuriyama, M. Gull, B. Moepps, M. Parsons and R. Mayor, *Dev Cell*, 2010, **19**, 39-53.
14. A. Dzementsei, D. Schneider, A. Janshoff and T. Pieler, *Biol Open*, 2013, **2**, 1279-1287.
15. J. D. Berndt, M. R. Clay, T. Langenberg and M. C. Halloran, *Developmental biology*, 2008, **324**, 236-244.
16. G. T. Charras, M. Coughlin, T. J. Mitchison and L. Mahadevan, *Biophys J*, 2008, **94**, 1836-1853.
17. G. T. Charras, C. K. Hu, M. Coughlin and T. J. Mitchison, *J Cell Biol*, 2006, **175**, 477-490.
18. A. Gautreau, D. Louvard and M. Arpin, *J Cell Biol*, 2000, **150**, 193-203.
19. P. Friedl and K. Wolf, *J Cell Biol*, 2010, **188**, 11-19.
20. G. T. Charras, J. C. Yarrow, M. A. Horton, L. Mahadevan and T. J. Mitchison, *Nature*, 2005, **435**, 365-369.
21. C. M. Franz and P. H. Puech, *Cel. Mol. Bioeng.*, 2008, **1**, 289-300.
22. T. Ludwig, R. Kirmse, K. Poole and U. S. Schwarz, *Pflugers Arch*, 2008, **456**, 29-49.
23. O. Chaudhuri, S. H. Parekh, W. A. Lam and D. A. Fletcher, *Nat Methods*, 2009, **6**, 383-387.
24. D. Alfandari, H. Cousin, A. Gaultier, B. G. Hoffstrom and D. W. DeSimone, *Dev Biol*, 2003, **260**, 449-464.
25. A. Borchers, H. H. Epperlein and D. Wedlich, *Dev Genes Evol*, 2000, **210**, 217-222.
26. F. Badique, D. R. Stamov, P. M. Davidson, M. Veuillet, G. Reiter, J. N. Freund, C. M. Franz and K. Anselme, *Biomaterials*, 2013, **34**, 2991-3001.
27. J. Hutter and J. Bechhoefer, *Review of Scientific Instruments*, 1993, **64**, 1868-1873.
28. M. Krieg, Y. Arboleda-Estudillo, P. H. Puech, J. Kafer, F. Graner, D. J. Muller and C. P. Heisenberg, *Nat Cell Biol*, 2008, **10**, 429-436.
29. R. Mayor and E. Theveneau, *Development*, 2013, **140**, 2247-2251.
30. M. R. Clay and M. C. Halloran, *Cell Adh Migr*, 2010, **4**, 586-594.
31. T. Gustafson and H. Kinnander, *Exp Cell Res*, 1956, **11**, 36-51.
32. D. R. McClay, J. R. Miller, C. Y. Logan, P. L. Hertzler, E. S. Bachman, J. C. Matese, D. R. Sherwood and N. A. Armstrong, *Theriogenology*, 1995, **44**, 1145-1165.
33. K. Hashimoto and N. Nakatsuji, *Development, Growth & Differentiation*, 1989, **31**, 209-218.